Environmental Science & Technology

Article

Cite This: Environ. Sci. Technol. 2018, 52, 9225−9234

pubs.acs.org/est

Parameterized Yields of Semivolatile Products from Isoprene Oxidation under Different NO_x Levels: Impacts of Chemical Aging and Wall-Loss of Reactive Gases

Li Xing,[†,‡,§] Manish Shrivastava,[*,‡] Tzung-May Fu,[*,†] Pontus Roldin,[∥] Yun Qian,[‡] Lu Xu,[⊥,#] Nga L. Ng,[⊥,▽] John Shilling,[‡] Alla Zelenyuk,[‡] and Christopher D. Cappa[○]

[†]Department of Atmospheric and Oceanic Sciences and Laboratory for Climate and Ocean-Atmosphere Studies, School of Physics, Peking University, Beijing 100871, China

[‡]Pacific Northwest National Laboratory, Richland, Washington 99352, United States

[§]Key Lab of Aerosol Chemistry & Physics, State Key Laboratory of Loess and Quaternary Geology, Institute of Earth Environment, Chinese Academy of Sciences, Xi'an 710061, China

[∥]Division of Nuclear Physics, Lund University, P.O. Box 118, 221 00 Lund, Sweden

[⊥]School of Chemical and Biomolecular Engineering, Georgia Institute of Technology, Atlanta, Georgia 30332, United States

[#]Division of Geological and Planetary Sciences, California Institute of Technology, Pasadena, California 91125, United States

[▽]School of Earth and Atmospheric Sciences, Georgia Institute of Technology, Atlanta, Georgia 30332, United States

[○]Department of Civil and Environmental Engineering, University of California, Davis, California 95616, United States

Supporting Information

ABSTRACT: We developed a parametrizable box model to empirically derive the yields of semivolatile products from VOC oxidation using chamber measurements, while explicitly accounting for the multigenerational chemical aging processes (such as the gas-phase fragmentation and functionalization and aerosol-phase oligomerization and photolysis) under different NO_x levels and the loss of particles and gases to chamber walls. Using the oxidation of isoprene as an example, we showed that the assumptions regarding the NO_x-sensitive, multigenerational aging processes of VOC oxidation products have large impacts on the parametrized product yields and SOA formation. We derived sets of semivolatile product yields from isoprene oxidation under different NO_x levels. However, we stress that these product yields must be used in conjunction with the corresponding multigenerational aging schemes in chemical transport models. As more mechanistic insights regarding SOA formation from VOC oxidation emerge, our box model can be expanded to include more explicit chemical aging processes and help ultimately bridge the gap between the process-based understanding of SOA formation from VOC oxidation and the bulk-yield parametrizations used in chemical transport models.

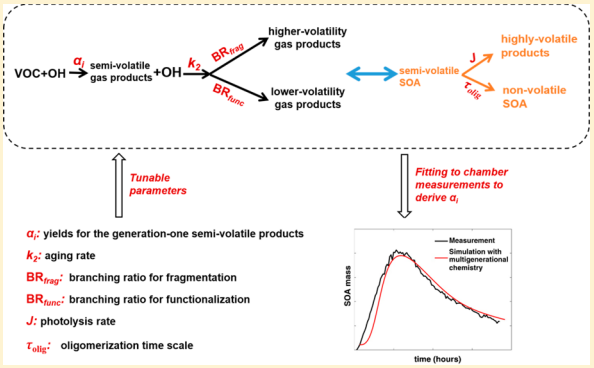

INTRODUCTION

Many volatile organic compounds (VOCs) oxidize in the atmosphere to produce lower volatility products that form secondary organic aerosols (SOA).[1−4] Laboratory studies have shown that the oxidation pathways of VOCs are sensitive to ambient NO_x levels, and that the molecular complexity and aging of VOC oxidation products have large impacts on the yields and formation time scales of SOA.[1−3,5,6] Many current chemical transport models simulated the SOA formation from VOC oxidation using parametrized yields derived from simple empirical theories.[7,8] At the same time, an increasing number of those same models are implementing complex chemical aging processes based on new mechanistic insights on SOA formation gained from laboratory studies.[9−11] This discrepancy between the implementation of detailed chemical mechanism and the use of simplified parametrized yields in models have so far been overlooked. Here, we presented a new way to parametrize the product yields from VOC oxidation using chamber measurements, taking isoprene oxidation as a specific example. We showed that the explicit accounting of chemical aging and chamber wall-loss processes changed the parametrized yields

Received: January 20, 2018
Revised: June 14, 2018
Accepted: July 20, 2018
Published: July 20, 2018

DOI: 10.1021/acs.est.8b00373
Environ. Sci. Technol. 2018, 52, 9225−9234

and volatility distribution of products, which will in turn affect the SOA simulation in chemical transport models.

The volatility basis set (VBS) framework, which expands on the two-product model,[12] is a widely used empirical approach for modeling SOA formation.[13−16] Under the VBS framework, a VOC precursor oxidizes to produce semivolatile and intermediate volatility (SV/IV) products, which are lumped into n (typically between 4 and 8) bins of effective volatility (represented by bins of effective saturation vapor concentration, C^*_i, i = 1 to n).[8,9,13] These SV/IV products then partition into the aerosol phase according to their respective volatility. To date, most studies parametrized the effective stoichiometric mass yields (α_i) of the SV/IV products by fitting to smog chamber measurements using eq 1,[7,8]

$$\xi \equiv \frac{\Delta C_{OA}}{\Delta ROG} = \sum_{i=1}^{n} \alpha_i \times \frac{1}{1 + \frac{C_i^*}{C_{OA}}} \quad (1)$$

where ξ was the aerosol mass fraction (AMF), which was the bulk yield of SOA mass from a reacted VOC precursor measured in the chamber. ΔROG was the reacted VOC precursor mass, and ΔC_{OA} was the total SOA mass formed (adjusted for particle wall-loss). C_i^* was the effective saturation vapor concentration of products in the volatility bin i, and C_{OA} was the total SOA mass. Typically, a series of experiments were performed by injecting different initial amounts of the VOC precursor into a chamber to be oxidized, and the values of ξ were calculated using the measured time series of the SOA mass and the reacted VOC mass. The product yields in different volatility bins (α_i, i = 1 to n) were then determined by fitting to the resulting series of ξ values.[8,9,17]

A frequently overlooked fact is that the yields empirically obtained from fitting eq 1 were theory-specific. It was assumed that (1) all wall-losses of particles during the measurement were accounted for prior to the fitting; (2) no SV/IV gases were lost to the walls; (3) the volatility of SV/IV products can be lumped into one single, static set of VBS products, which allowed no evolution of their volatility by chemical aging; and (4) the gas/aerosol partitioning of the SV/IV products followed the absorptive partitioning theory. Recent laboratory results have shown that these assumptions pertaining to eq 1 may not apply.[1,18−20] For example, SV/IV gases might be lost to chamber walls during the experiments, leading to a factor of 2 to 10 underestimation of the product yields, especially when the seed-to-chamber surface area ratio was relatively low,[21−23] although SOA mass yields may not be affected by vapor wall-loss if the SOA formation was governed by fast quasi-equilibrium growth on seed particles.[24]

More importantly, the product yields parametrized from eq 1 were based only on the total SOA mass formed, with little relevance to the changes of volatility distribution due to aging either within or beyond the chamber experiment time scale (typically a few hours). In reality, the SV/IV products from VOC oxidation undergo mutigenerational aging processes that were highly sensitive to NO_x, within the time scale of the chamber experiments and also beyond,[1,19] leading to significant changes in volatility and thus SOA yields. For example, under low-NO_x (HO_2-dominant) conditions, chamber experiments of isoprene oxidation showed that SOA mass began to decline once all isoprene was consumed.[1,5] This decline of SOA mass may be due to the photolysis of hydroperoxides in the aerosol phase, or the evaporation of SOA mass once gas-phase compounds were reacted away.[5,6] At the same time, the mean SOA oxidation state (represented by 2O/C−H/C)[25] continued to increase during an 18-h experiment under low-NO_x conditions,[1] indicating the formation of highly oxidized (and potentially less volatile) molecules containing one or more peroxy, hydroxyl, or carbonyl function groups.[1,26−28] However, in chamber experiments under high-NO_x conditions, SOA mass continued to increase even after all the isoprene has reacted. The mean oxidation state of SOA was higher than that of low-NO_x experiment and remained nearly constant during an 18-h experiment under high-NO_x conditions.[1]

Several model studies have tried to incorporate these new mechanistic insights gained from chamber experiments to improve the simple VBS n-product scheme.[15,16,23,29] One way to do this was to allow the generation-one VBS products to further oxidize and undergo functionalization/fragmentation at assumed branching ratios.[15,16] This approach allowed the formation of higher-generation oxidation products with evolving volatility profiles.[15,29] In so doing, the great complexity of the multigenerational aging of thousands of oxidation products was reduced and represented with a small set of lumped VBS products. To date, models using such VBS-plus-aging schemes have used products yields empirically obtained from eq 1 and added subsequent multigenerational aging processes.[15,16] However, if multigenerational aging was not included during the parametrization of product yields, then it could bias the product yields that serve as initial concentrations for subsequent chemistry. Consequently, there is strong potential for the VBS-plus-aging schemes to overestimate SOA.[29,30]

In this study, we constructed a box model that included multigenerational chemistry of isoprene oxidation and the losses of gas and particles to chamber walls. We then ran the box model with different chemical aging scenarios to fit the measured time series of SOA mass concentrations from chamber experiments under different NO_x level. In this way, we investigate the effects of chemical aging and gas wall losses on the parametrized yields and SOA formation from isoprene.

METHODOLOGY

Chamber Experiment Results from Xu et al.[1] We used the time series of SOA mass concentrations in the isoprene oxidation experiments by Xu et al.,[1] which were conducted in the Pacific Northwest National Laboratory (PNNL) dual 10.6 m^3 Teflon environmental chambers with different initial concentrations of isoprene and NO_x. The chambers were flushed with pure air prior to each experiment and no seed particles were used. UV lamps initiated the photochemical reactions. A proton transfer reaction mass spectrometer (PTR-MS) measured the concentrations of isoprene and two of its major oxidation products, methacrolein (MACR) and methyl vinyl ketone (MVK). A scanning mobility particle sizer (SMPS) measured the aerosol size distribution between 14.1 and 710.5 nm every 5 min. SOA mass concentrations were calculated from the aerosol volume concentrations measured by the SMPS, assuming particle densities of 1.3 g cm^{-3} (experiment 2) and 1.4 g cm^{-3} (experiments 6 and 8). We analyzed results from three experiments with different initial NO/isoprene ratios: ∼0, 3.0, and 7.3 (experiments 2, 6, and 8 in Xu et al.[1]) to examine the impact of NO_x. In experiment 2, the NO_x concentration was below the detection limit (1 ppb) throughout the experiment, such that organic peroxy radicals (RO_2) mainly reacted with HO_2; this was referred to as an "HO_2-dominant" experiment. In experiments 6 and 8, NO was injected into the chambers and RO_2 radicals may react with HO_2, NO, and NO_2. We referred

DOI: 10.1021/acs.est.8b00373
Environ. Sci. Technol. 2018, 52, 9225−9234

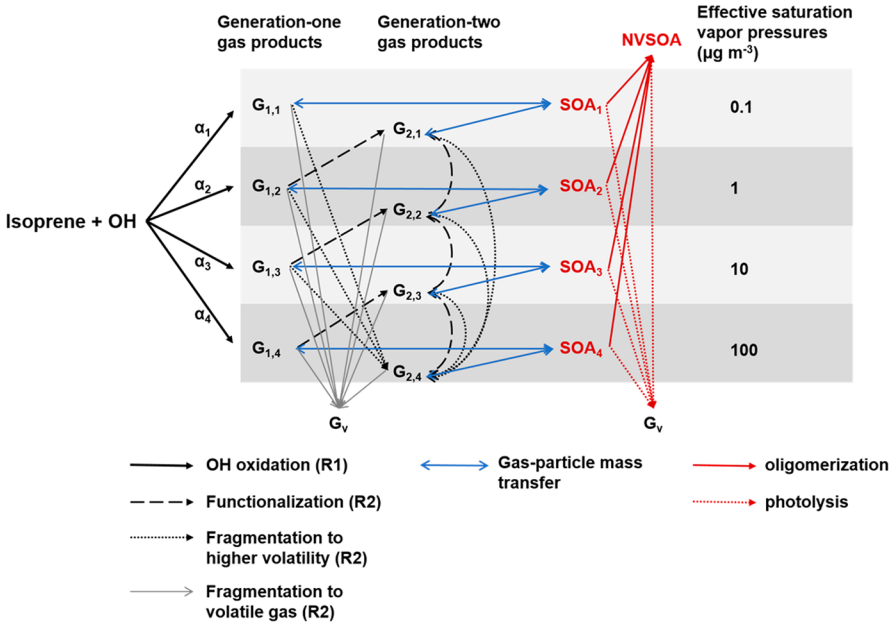

Figure 1. Schematic of the box model describing the multigenerational chemistry of isoprene oxidation leading to SOA formation.

to experiments 6 and 8 as "intermediate-NO_x mixed" and "high-NO_x mixed" experiments, respectively. Measurements from the other five experiments in Xu et al.[1] were used for validation (Supporting Information, SI).

Box Model for SOA Formation from Isoprene Oxidation. We constructed a parametrizable box model to simulate the oxidation of isoprene and the subsequent multigenerational chemistry of the gas and aerosol products. Our box model was built on the framework of the Model for Simulating Aerosol Interactions and Chemistry (MOSAIC),[31] which was a discretized-size-bin model originally developed to describe the chemical and microphysical evolution of inorganic aerosols. Here we included a multigenerational aging scheme for isoprene oxidation using the modified VBS aging scheme developed by Shrivastava et al.[15] Figure 1 and Table S1 show the gas- and aerosol-phase reactions and gas-particle mass transfer pathways in the model. Isoprene reacts with OH (reaction R1, rate constant $k_1 = 1.0 \times 10^{-10}$ cm^3 molecule^{-1} s^{-1})[32] to produce generation-one semivolatile gas products ($G_{1,i}$, i = 1 to 4) in four effective saturation vapor concentration bins (C^*_i, i = 1 to 4): 0.1, 1, 10, and 100 μg m^{-3} at yields α_i (i = 1 to 4), respectively. Some intermediate-volatility products with saturation vapor concentrations between 10^3–10^5 μg m^{-3} may potentially oxidize to form SOA.[33] However, the maximum SOA concentration measured during the experiments by Xu et al.[1] was <25 μg m^{-3}; thus there will be large uncertainty when interpreting the yields for products with saturation vapor concentrations exceeding 10^3 μg m^{-3}, as less than 3% of those products partitioned into the particle phase.[13] Note that the generation-one products here refer to the lumped semivolatile products in the VBS framework; they do not directly correspond to specific first-generation products from isoprene oxidation, such as MACR, MVK, or isoprene hydroxy-hydroperoxides (ISOPOOH).

We assumed that the generation-one products may react with OH (reaction R2, rate constant $k_2 = 2.0 \times 10^{-11}$ cm^3 molecule^{-1} s^{-1})[34] to form generation-two products ($G_{2,i}$, i = 1 to 4) with one of three chemical transformation branches: (1) some products fragmented to form generation-two products in the highest volatility bin (from $G_{1,i}$ to $G_{2,4}$, i = 1 to 4) (quantified by a branching ratio BR_{frag}); (2) some products functionalized to form generation-two products in a volatility bin that is one lower (from $G_{1,i}$ to $G_{2,i-1}$, i = 2,3,4) (branching ratio BR_{func}) with a 15% mass increase due to the added oxygen; and (3) 10% of the product formed highly volatile gases (G_v), which no longer contribute to SOA formation. Generation-two products were also assumed to undergo similar aging processes to form generation-three products. The higher generation products were lumped into the generation-two products to reduce computation cost.

The rate of mass growth for SOA particles of diameter D_p in the i^{th} volatility bin $\left(\frac{dSOA_i(D_p)}{dt}\right)$ due to diffusive condensation of generation-j gases in the i^{th} volatility bin was calculated as follows:[35]

$$\frac{dSOA_i(D_p)}{dt} = \sum_i 2\pi D_{gas} D_p \left(C_{j,i} - C^*_{j,i} \exp\left(\frac{4\sigma M_i}{RT\rho D_p}\right)\chi_i\right) f(Kn, a) \quad (2)$$

where $C_{j,i}$ and $C^*_{j,i}$ were the gas phase concentration and saturation vapor concentration of organic product $G_{j,i}$, respectively. σ was the particle surface tension (0.05 N m^{-1}),[36] M_i was the molecular weight of the organic species in the i^{th} volatility bin (assumed to be uniformly 250 g mol^{-1}), D_{gas} was the diffusion coefficient of the organic species in air (set to a constant of 0.05 cm^2 s^{-1}),[37] R was the universal gas constant, T was the temperature (K), ρ was the particle density (1 g cm^{-3}), χ_i was the mole fraction of the i^{th} volatility-bin species in the particle phase. $f(Kn,a)$ was the correction factor for noncontinuum conditions (SI).[38]

We further assumed that species in the condensed phase may undergo either one or two types of chemical transformation: (1) slow oligomerization of the semivolatile SOA to form nonvolatile, nonabsorptive SOA (NVSOA) on a time scale (τ_{olig}) of 20 h[39] or a time scale of 10 min[40] (first order rate constant $k_{olig} = 1/\tau_{olig}$); and/or (2) all condensed organics may photolyze to form highly volatile species (beyond the SV/IV range), with an assumed photolysis frequency of $J = 3.2 \times 10^{-6}$ s^{-1}.[41] Aerosols were assumed to be internally mixed

DOI: 10.1021/acs.est.8b00373
Environ. Sci. Technol. 2018, 52, 9225−9234

within each of the 50 size bins. The particle size changes due to diffusive condensation/evaporation and Brownian coagulation were simulated using the moving-section approach.[42,43]

We explicitly accounted for the loss of particles and reactive gases to the chamber walls in our box model. The loss of particles to the chamber walls was characterized by a size-dependent, first-order deposition rate.[44] We tuned this particle deposition rate in our box model to match the particle number concentration and size distribution measurements from a separate ammonium sulfate particle deposition experiment by Xu et al.[1] We assumed the deposition of semivolatile organic gases to chamber walls to be irreversible.[21,22,45] The first-order deposition frequency of a semivolatile gas was calculated as a function of the eddy diffusion coefficient in the chamber and the mass accommodation coefficient of the semivolatile gas on the wall.[22] In turn, the mass accommodation coefficient of a semivolatile gas on the wall was a function of its volatility,[22] which we tuned for the PNNL chamber. Further details about the particle and gas wall-loss calculations are given in the SI.

Chemical Scenarios and Fitting Procedure. We designed model experiments with eleven chemical scenarios, each with a different combination of chemical aging processes in the gas and particle phases and wall-loss treatments. Table 1 describes the chemical scenarios (scenarios 1 to 11). The simplest, "Non-aging_noGL" scenario assumed that no chemical transformation took place in either the gas or particle phase beyond the production of the generation-one products, and that no reactive gases were lost to the walls. Then, the wall-loss of semivolatile species was turned on in a "Non-aging" scenario. Keeping the wall-loss of semivolatile gases turned on, we further experimented with different configurations of multigenerational chemistry in the gas-phase by setting the branching ratios for fragmentation and functionalization (BR_{frag}, BR_{func}) to (0.25, 0.65), (0.5, 0.4), or (0.75, 0.15), respectively. In addition, we experimented with different configurations of particle-phase chemistry: slow oligomerization of semivolatile SOA to form NVSOA, as well as inclusion/exclusion of SOA photolysis.

We fitted our box model to the observed time series of SOA masses under different levels of NO_x using a two-step procedure, using the generation-one product yields (α_i) as tunable parameters. First, for each chemical scenario, we varied each of the four generation-one product yields between 10^{-5} to 10^{-1} with 40 logarithmic increments, performing 40^4 = 2 560 000 model realizations. For each model realization, we ran the model to oxidize isoprene (OH concentration was constrained by the measured isoprene decay rate) assuming the gas phase chemistry of that scenario and gas wall-loss turned on for a short period of initialization time (t_0 = 0.75, 1, and 3 h for experiments 2, 6, and 8 in Xu et al.,[1] respectively). By these t_0 times, the SMPS could measure the aerosol size distribution between 14.1 and 710.5 nm in the chamber. From t_0 onward, we assumed that the SMPS-observed aerosol size distributions at t_0 served as de facto aerosol seeds, which were inert and would not subsequently evaporate or chemically age. We then used the simulated gaseous product concentrations at t_0 as initial conditions and restart the model from t_0 to simulate the isoprene oxidation chemistry using the consistent chemical scenario and α_i values. We computed the sum-of-squared differences between measured and simulated time series of SOA concentrations from the initialization time (t_0) to the end of experiment (18, 18, and 14 h for experiments 2, 6, and 8 in Xu et al.,[1] respectively). The model realization with the least

Table 1. Design of Model Chemical Scenarios

	chemical scenarios	gas-phase chemical transformation	aerosol-phase chemical transformation	wall-loss of semivolatile gases[a]
1	non-aging_noGL	no chemical aging of the generation-one semivolatile from isoprene oxidation	no chemical aging in the aerosol phase	gas wall-loss module turned off
2	Non-aging	same as in non-aging_noGL	same as in non-aging_noGL	gas wall-loss module turned on
3/4/5	FragH_OligS_P/FragM_OligS_P/FragL_OligS_P	generation-one semivolatile products were oxidized to produce generation-two products with BR_{frag} = 0.75 (H)/0.5 (M)/0.25 (L) and BR_{func} = 0.15 (H)/0.4 (M)/0.65 (L), respectively	semivolatile SOA mass oligomerized to form nonvolatile SOA (NVSOA) on a time scale of 20 h (k_{olig} = 1.39× 10^{-5} s^{-1}). at the same time, semivolatile SOA and NVSOA mass were removed by photolysis (J = 3.2 × 10^{-6} s^{-1}).	gas wall-loss module turned on
6/7/8	FragH_OligS/FragM_OligS/FragL_OligS	same as the gas phase chemistry in FragH_OligS_P/FragM_OligS_P/FragL_OligS_P	semivolatile SOA mass oligomerized to form NVSOA on a time scale of 20 h (k_{olig} = 1.39× 10^{-5} s^{-1}). no photolysis of SOA.	gas wall-loss module turned on
9/10/11	FragH_OligF_P/FragM_OligF/FragL_OligF	same as the gas phase chemistry in FragH_OligS_P/FragM_OligS_P/FragL_OligS_P	semivolatile SOA mass oligomerized to form NVSOA on a time scale of 10 min (k_{olig} = 1.67 × 10^{-3} s^{-1}). semivolatile SOA and NVSOA mass were removed by photolysis (J = 3.2 × 10^{-6} s^{-1}) in FragH_OligF_P. no SOA photolysis in FragM_OligF and FragL_OligF.	gas wall-loss module turned on

[a]The particle wall-loss module was turned on for all chemical scenarios.

DOI: 10.1021/acs.est.8b00373
Environ. Sci. Technol. 2018, 52, 9225−9234

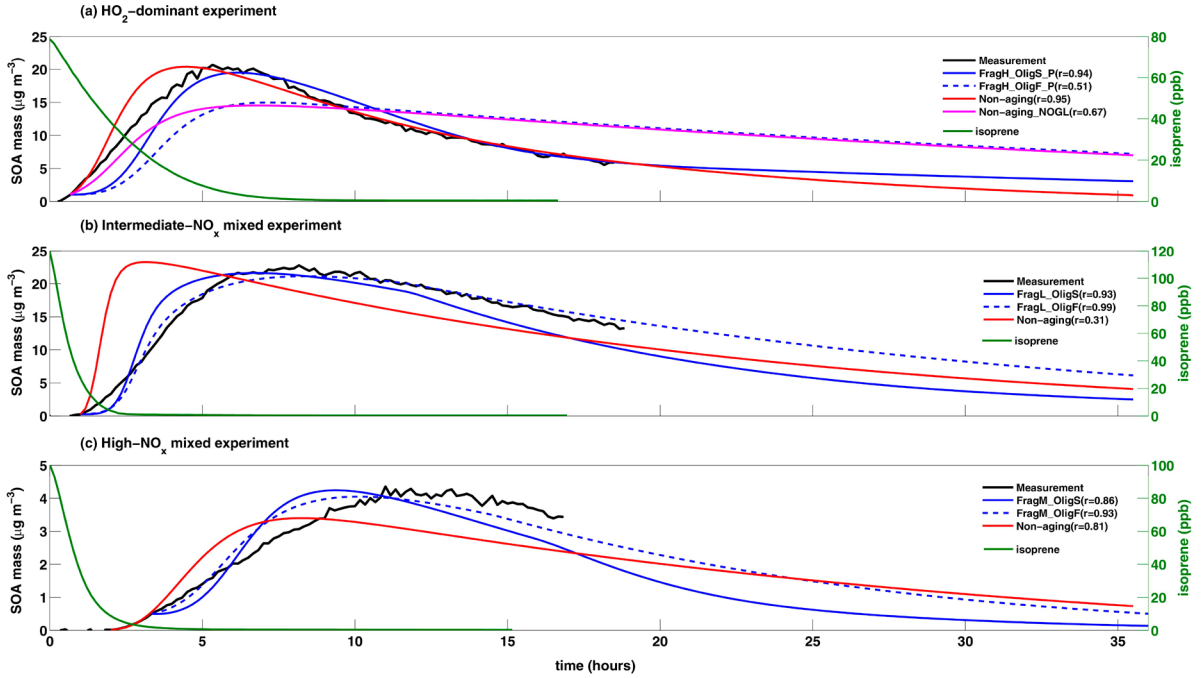

Figure 2. Observed (black) and simulated time series of SOA mass and the isoprene concentrations (green) for the (a) HO_2-dominant, (b) intermediate-NO_x, and (c) high-NO_x mixed experiments conducted by Xu et al.[1] The simulated time series of SOA mass that best-fitted the observations under different chemical scenarios are shown. The correlation coefficients between the observed and simulated time series are shown in parentheses.

Table 2. Best-Fit Chemical Scenarios and Product Mass Yields for the HO_2-Dominant, Intermediate-NO_x, and High-NO_x Mixed Experiments, and Comparison with the Yields in the Literature Used by Chemical Models

	C* (μg m^{-3})			
experiments (chemical scenarios)	0.1	1	10	100
HO_2-dominant experiment (FragH_OligS_P)	3.68×10^{-5}	5.52×10^{-4}	2.82×10^{-1}	6.44×10^{-2}
HO_2-dominant experiment (Non-aging)	6.26×10^{-4}	2.65×10^{-2}	1.73×10^{-2}	2.43×10^{-1}
intermediate-NO_x mixed experiment (FragL_OligS)	3.68×10^{-5}	3.68×10^{-5}	1.80×10^{-3}	2.50×10^{-1}
intermediate-NO_x mixed experiment (FragL_OligF)	1.80×10^{-3}	2.61×10^{-4}	1.80×10^{-3}	2.18×10^{-1}
high-NO_x mixed experiment (FragM_OligS)	3.68×10^{-5}	3.68×10^{-5}	3.68×10^{-5}	2.44×10^{-1}
high-NO_x mixed experiment (FragM_OligF)	3.68×10^{-5}	3.68×10^{-5}	3.68×10^{-5}	2.34×10^{-1}
literature[a]				
HO_2-dominant experiment[a]	0.0	6.00×10^{-3}	2.00×10^{-2}	1.00×10^{-2}
intermediate-NO_x mixed experiment[a]	0.0	3.10×10^{-3}	1.75×10^{-2}	1.00×10^{-2}
high-NO_x mixed experiment[a]	0.0	2.00×10^{-4}	1.5×10^{-2}	1.00×10^{-2}

[a]Product yields in the literature were derived assuming no chemical aging by fitting to eq 1 and were used by the WRF-Chem and PMCAMx models.[14,15]

sum-of-squared difference was selected to indicate the best-fit generation-one product yields for that specific chemical scenario.

RESULTS AND DISCUSSION

Yields of Semivolatile Products from Isoprene Oxidation for HO_2-Dominant Experiment. We began by investigating the SOA formation from isoprene oxidation for the HO_2-dominant experiment, guided by the mechanistic insights indicated by previous chamber studies.[1,5] Experiments showed that OH-oxidation of isoprene produced ISOPOOH as the major first-generation product under HO_2-dominant environments.[46] Oxidation of ISOPOOH by OH mainly produced isoprene epoxydiols ($CH_2OHC(CH_3)OCHCH_2OH$, hereafter IEPOX) by functionalization. IEPOX reacted with OH to form organic peroxides and polyols, as well as smaller products such as formic acid, acetic acid, glycolaldehyde, and hydroxyacetone.[47] In the aerosol phase, oligomers (mostly dimers) have been detected in similar experiments.[18] The hydroperoxides in SOA may photolyze, or the gas-phase compounds may fragmentize and the corresponding SOA mass evaporate to the gas phase, which both could result in the observed fast decay of SOA mass.[5,6] Given these observational constraints, we experimented with chemical scenarios including multigenerational gas chemistry and aerosol-phase oligomerization and photolysis.

Figure 2(a) shows the measured time series of SOA mass during the HO_2-dominant experiment in Xu et al.,[1] as well as the simulated time series of SOA mass that best fitted the measurements assuming different chemical scenarios. Table 2 compares the generation-one product yields obtained from the fitting under different chemical scenarios. The best fit against measurements was obtained assuming nonaging of the gaseous

DOI: 10.1021/acs.est.8b00373
Environ. Sci. Technol. 2018, 52, 9225−9234

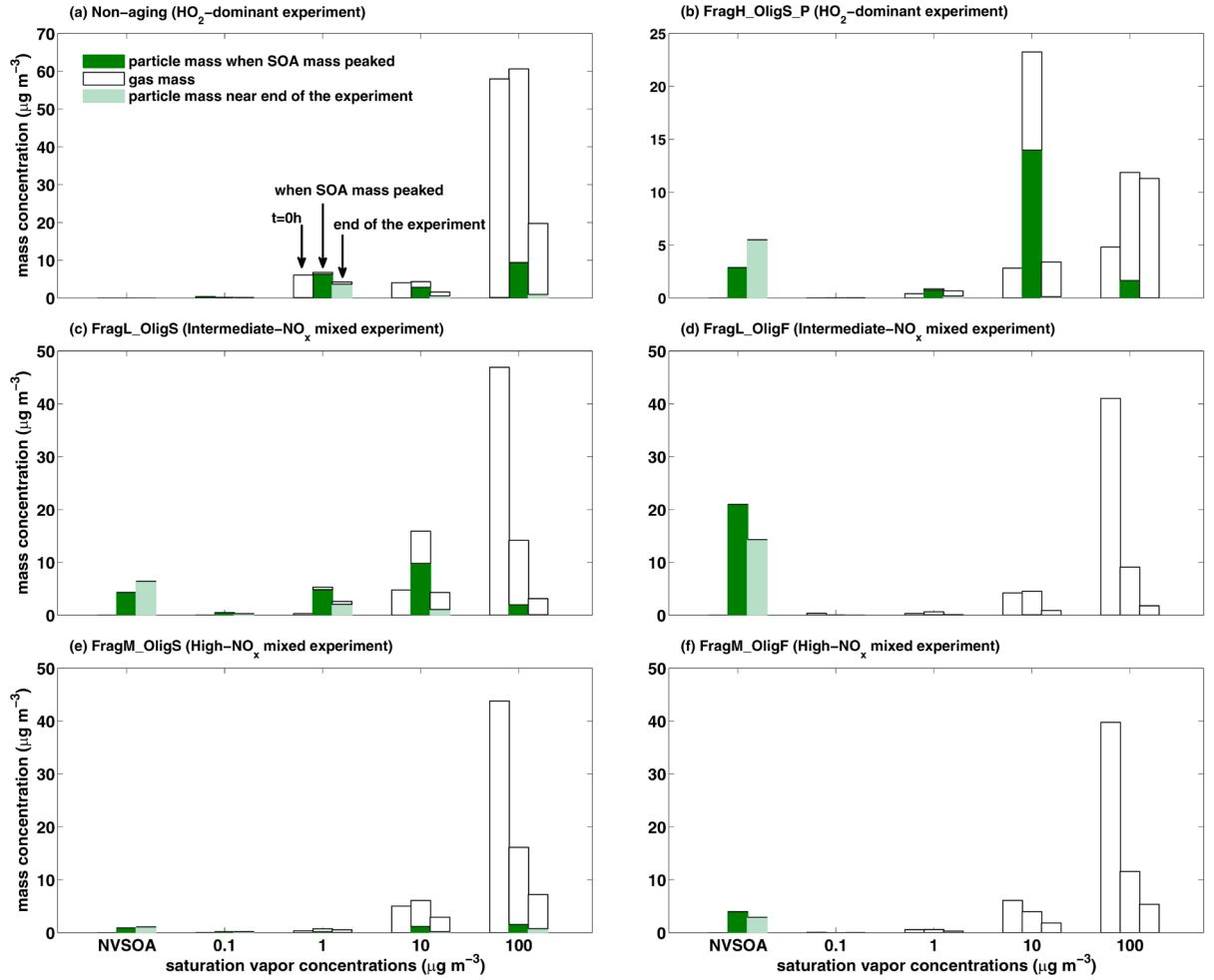

Figure 3. Simulated product mass distributions under specific chemical scenarios under different NO_x conditions. For HO_2-dominant experiment: (a) the Non-aging scenario and (b) the FragH_OligS_P scenario; for intermediate-NO_x mixed experiment: (c) the FragL_OligS scenario and (d) the FragL_OligF scenario; for high-NO_x mixed experiment: (e) the FragM_OligS scenario and (f) the FragM_OligF scenario. For each simulation, the product masses at $t = t_0$, at time when SOA mass peaked, and at a time near the end of the experiment are shown. The white bars represent the gas phase concentrations in each volatility bin. The green bars represent aerosol phase concentrations when SOA mass peaked (dark green) and near the end of the experiments (light green).

and aerosol products (Non-aging scenario, $r = 0.95$). A good fit was also obtained under the FragH_OligS_P sceneario ($r = 0.94$), which assumed multigenerational gas-phase chemistry with $BR_{frag} = 0.75$ and $BR_{func} = 0.15$, slow SOA oligomerization ($\tau_{olig} = 20$ h), and SOA photolysis. Chemical scenarios with lower fragmentation branching ratios were unable to fit the measurements. The high BR_{frag} value in our best-fit scenario is somewhat contradictory to the experimental indication of organic peroxides and polyols (both highly functionalized) as the major products from IEPOX oxidation in the HO_2 experiments.[48] However, we stress that the fragmentation branching ratio, as implemented in our box model, represents an effective ratio for the overall fragmentation of the lumped, multigeneration VBS products. In addition, the high best-fit BR_{frag} may compensate for the oligomerization of SOA and/or the lower volatility range in our VBS framework.

The simulated evolutions of SOA mass under the two best-fit scenarios were different (Figure 2(a)). Between t_0 (0.75 h) and the time when measured SOA mass peaked (5 h), the FragH_OligS_P simulation underestimated the observed SOA mass while the Non-aging simulation overestimated the observed SOA mass. During the remainder of the experiment and for simulation times beyond the experiment, the simulated SOA mass under the FragH_OligS_P scenario decayed slower than that simulated under the Non-aging scenario. Table 2 showed that the generation-one semivolatile product mass was mostly in the $C^* = 10$ μg m^{-3} bin for the FragH_OligS_P scenario but mostly in the $C^* = 100$ μg m^{-3} bin for the Nonaging scenario.

To understand the differences between the Non-aging and FragH_OligS_P simulations, we examined the simulated product mass distributions under the two chemical scenarios at $t = t_0$, $t = 5$ h (when SOA mass peaked), and $t = 18$ h (end of the experiment), respectively (Figure 3(a, b)). In the FragH_OligS_P simulation, initially the semivolatile gases were mostly in the higher volatility bins due to the larger yields. By $t = 5$ h, a fraction of the semivolatile product mass was moved to the $C^* = 10$ μg m^{-3} bin by gas-phase functionalization. During the latter part of the FragH_OligS_P simulation ($t = 18$ h), SOA mass decayed due to the loss of semivolatile gases to chamber walls, but this decay was relatively slow due to the oligomerization of semivolatile SOA to from NVSOA. The loss of SOA mass via photolysis of aerosol-phase products was less important, as evidenced by a sensitivity simulation using the best-fit

DOI: 10.1021/acs.est.8b00373
Environ. Sci. Technol. 2018, 52, 9225−9234

yields of FragH_OligS_P scenario with photolysis turned off (Figure S8). In contrast, under the Non-aging scenario, SOA was formed at the beginning of the simulation by condensation of semivolatile products. To suppress wall-loss of gases, most of the generation-one product mass was distributed in the highest volatility bin (C^* = 100 μg m^{-3}). This mass distribution of products was relatively stable with respect to time, because no chemical aging took place. As a result, during the latter part of the simulation, organic mass was more rapidly lost to the walls compared to the FragH_OligS_P simulation, and SOA mass quickly decayed.

Our analyses above showed that including the multigenerational gas-phase chemistry and aerosol-phase reactions explicitly during the fitting changed the parametrized product yields and the simulated SOA mass evolution over a long time-scale, even for HO_2-dominant experiment where the chemistry was relatively simple.

Yields of Semivolatile Products and SOA from Isoprene Oxidation for Mixed Experiment. In isoprene photooxidation experiments with NO injected into the chambers, MACR were found to be the main first-generation products leading to SOA formation.[1,6] The peroxy radical of MACR ($MACRO_2$) may react with NO, forming products that further fragmented into volatile species (such as hydroxyacetone and methylglyoxal) and resulted in inefficient SOA formation.[49,50] Alternatively, $MACRO_2$ may react with NO_2 to form methacryloylperoxynitrate (MPAN), which could be further oxidized and functionalized to form 2-methylglyceric acid (2-MG).[51] Thus, fragmentation and functionalization reactions can have large impacts on the SOA yields in the mixed experiments, and their relative contributions depend on the NO/NO_2 ratio. Oligomerization with three and four monomer units were observed during mixed experiments.[6,18] SOA photolysis was not observed to be significant in mixed experiments.[1,5] Given these experimental constraints, we simulated with multigenerational gas-phase chemistry using different combinations of fragmentration/functionalization branching ratios, as well as aerosol oligomerization to fit the measurements.

Figure 2(b, c) showed the measured time series of SOA mass, as well as the simulated time series that best fitted the measurements for the intermediate-NO_x and high-NO_x mixed experiments, respectively. For the intermediate-NO_x mixed experiment, the simulation with BR_{frag}= 0.25 and BR_{func} = 0.65 fitted the measurements best (FragL_OligS scenario, r = 0.93). For the high-NO_x mixed experiment, best-fit was found with BR_{frag} = 0.5 and BR_{func} = 0.4 (FragM_OligS scenario, r = 0.86). These fitting results indicated that higher initial NO concentrations led to more fragmentation of isoprene oxidation products, which corroborated the experimental evidence of enhanced fragmentation and delayed SOA formation under higher initial NO levels.[1,52] Sensitivity simulations using the Non-aging scenario were unable to reproduce the observed evolution of SOA mass. This was consistent with the observation that, for mixed experiments, SOA mass started to increase only after nearly all isoprene was consumed,[1] which indicates that SOA were composed of second and/or later generation products.

Table 2 compares the best-fit generation-one product mass yields for intermediate-NO_x and high-NO_x mixed experiments. The two mixed experiments both produced most of the generation-one product mass in the C^* = 100 μg m^{-3} bin. This was because SOA mass formation was delayed in the presence of NO_x, such that the fitting suppressed initial SOA formation by forming generation-one products mass in the highest volatility bin. The product yield at C^* = 10 μg m^{-3} were substantially higher for the FragL_OligS scenario in the intermediate-NO_x mixed experiment than that for the FragM_OligS scenario in the high-NO_x mixed experiment. This resulted in higher overall SOA production from isoprene oxidation under intermediate-NO_x conditions than under high-NO_x conditions (Figure 3(c) and 3(e)).

Impacts of the Rate of Oligomerization on Product Yields. We took the chemical scenarios that best-fitted the measurements for the HO_2-dominant and mixed experiments and accelerated the oligomerization, such that semivolatile SOA oligomerize to form NVSOA on a time scale of 10 min.[40] The best-fit results for these three additional chemical scenarios (FragH_OligF_P, FragL_OligF, and FragM_OligF; scenarios 9 to 11 in Table 1) are shown in Figure 2 and Table 2. We found that the FragH_OligF_P scenario did not fit the observed time series of SOA mass for the HO_2-dominant experiment (r = 0.51). For the intermediate-NO_x and high-NO_x mixed experiments, the simulations assuming fast oligomerization produced better fitting results with the observed time series of SOA mass than those assuming slow oligomerization, especially during the decaying stage of SOA mass. This is consistent with experimental evidence indicating more extensive oligomerization in mixed experiments than in HO_2-dominant experiments.[18] Figure 3(d, f) showed that fast oligomerization resulted in most of SOA mass being moved to NVSOA for the mixed experiments. The assumption of faster SOA oligomerization increased the best-fit product yields at C^* = 0.1 and 1 μg m^{-3} for the intermediate-NO_x mixed experiments, which suppressed SOA formation during the early stages of the experiment by increasing gas wall-loss. The best-fit product yields for the high-NO_x experiment did not change significantly when different oligomerization rates were applied. This was likely because the high-NOx experiment was conducted for a shorter period of time, such that there was insufficient observational constraint on the SOA mass evolution at longer time scales (Figure 2(c)).

Impact of Gas Wall-Loss on Yields. We investigated the impacts of gas wall-loss to the generation-one product yields by conducting a simulation for HO_2-dominant experiment with no gas/aerosol phase aging and no loss of gases to walls (Non_aging_noGL scenario) but found the model unable to fit the observed time series of SOA mass (Figure 2(a), r = 0.67). The simulation underestimated SOA mass during the first 10 h but grossly overestimated the measured SOA mass at longer times, as semivolatile gases was retained in the model. By accounting for the wall-loss of reactive gases during the fitting of product yields using chamber SOA measurements, the parametrized overall semivolatile organic mass yield was increased from 4.3% to 6.7%, which will in turn enhance the simulated atmospheric SOA concentrations in chemical transport models.[22,23]

Simulated Atmospheric SOA Concentrations Using Our Best-Fit Chemical Scenarios and Product Yields and Implications for Chemical Transport Models. We simulated atmospheric SOA concentrations from isoprene oxidation by applying our best-fit chemical scenarios and semivolatile product yields under different NO_x levels, the results are shown in Figure 4. To simulate atmospheric SOA concentrations, we turned off the gas and particle wall-loss calculations in our model and set a dilution rate of 6% per hour to represent the dilution of gas and particle concentrations due to mixing with ambient air.[15]

DOI: 10.1021/acs.est.8b00373
Environ. Sci. Technol. 2018, 52, 9225−9234

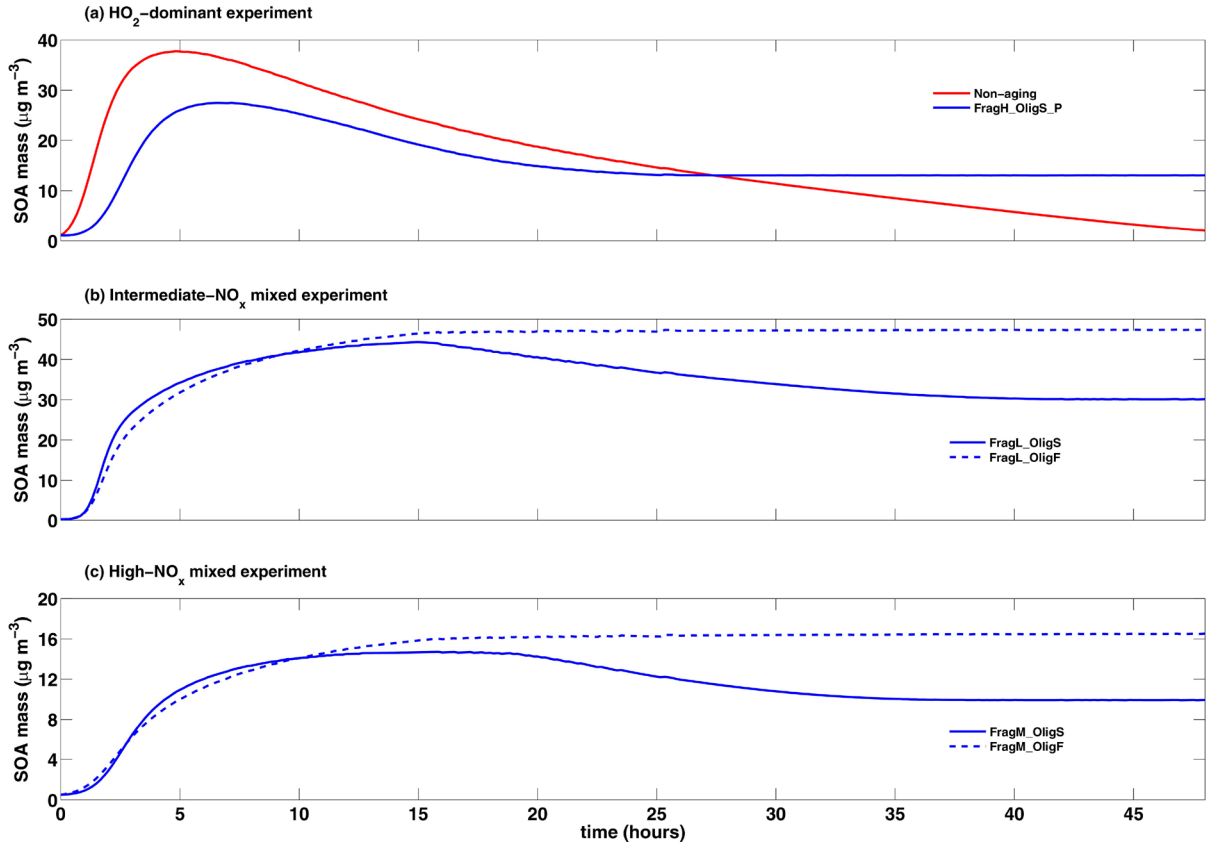

Figure 4. Simulated concentrations of atmospheric SOA from isoprene oxidation using our best-fit chemical scenarios/product yields under different levels of NO_x: (a) the HO_2-dominant experiment; (b) the intermediate-NO_x mixed experiment; and (c) the high-NO_x mixed experiment.

Under HO_2-dominant conditions, the simulated atmospheric SOA concentrations using the best-fit Non-aging scenario/yields were higher than that of the FragH_OligS_P scenario/yields during the first 26 h. In chamber fitting under the Non-aging scenario, the loss of SOA mass at long simulation time was mostly gas and particle wall-loss. Thus, the simulated atmospheric SOA concentrations would be higher when the gas and particle wall-losses were turned off. Accounting for multigenerational chemistry in the gas phase and oligomerization/photolysis in the aerosol phase (FragH_OligS_P scenario) slowed SOA formation rate in the first few hours and decreased the peak SOA mass. After the first 26 h, much of the semivolatile SOA have oligomerized to NVSOA in the FragH_OligS_P scenario, such that the decay rate of SOA mass slowed and high SOA concentrations was sustained.

In the presence of NO_x, initially the simulated atmospheric SOA concentrations were similar regardless of the assumptions of SOA oligomerization rates. Beyond the first 15 h or so, the SOA concentrations remained relatively constant in the fast oligomerization scenarios, while the SOA concentrations for the slow oligomerization scenarios gradually decreased. This was because fast oligomerization transformed most of the semivolatile SOA mass to NVSOA after only 15 h, such that less organic mass was lost to fragmentation. Thus, the rate at which SOA oligomerize have large impacts on the fate of atmospheric SOA. At present, it remains difficult to determine what oligomerization rates are appropriate for isoprene oxidation product under different levels of NO_x. Xu et al.[1] conducted thermal denuder measurements to quantify the volatility of SOA from isoprene oxidation. However, we were unable to use those measurements to constrain the choice of oligomerization rates due to uncertainty in the thermal stability of the oligomers,[53,54] which will be explored in a future work.

We presented above a new way to parametrize the yields of semivolatile products from VOC oxidation (using isoprene as an example), while explicitly accounting for the multigenerational chemical aging processes under different NO_x levels and the loss of particles and gases to chamber walls. We found that the assumptions regarding the multigenerational aging processes have large impacts on the parametrized product yields. It is therefore important that the SOA formation mechanisms implemented in chemical transport models be driven by product yields that were derived from consistent SOA formation pathway assumptions. The details of many multigenerational aging processes leading to SOA formation (such as gas-phase fragmentation/functionalization, aerosol-phase oligomerization, and photolysis), are still poorly understood and need to be better constrained in the laboratories. As more mechanistic insights regarding SOA formation from VOC oxidation emerge, our box model can be expanded to include more explicit chemical aging processes and help ultimately bridge the gap between the process-based understanding of SOA formation from VOC oxidation and the bulk-yield parametrizations used in chemical transport models.

■ ASSOCIATED CONTENT

Supporting Information

. The Supporting Information is available free of charge on the ACS Publications website at DOI: 10.1021/acs.est.8b00373.

Details about the calculations of diffusive condensation/evaporation of semivolatile species (Section S1), the

DOI: 10.1021/acs.est.8b00373
Environ. Sci. Technol. 2018, 52, 9225−9234

wall-loss of particles (Section S2), and semivolatile gases (Section S3); comparison of simulated particle size distribution against measurements (Section S4); validation of best-fit chemical scenarios/product yields against additional chamber experiments (Section S5); impacts of gas-phase chemical aging rates and aerosol oligomerization rates on the parametrized yields (Section S6); impacts of wall-loss of semivolatile gases and aerosol photolysis on the SOA simulation (Figure S8); and as and aerosol-phase reactions in the box model (Table S1) (PDF)

AUTHOR INFORMATION

Corresponding Authors

*Phone: 509-371-6792. E-mail: ManishKumar.Shrivastava@pnnl.gov (M.S.).

*Phone: +86-10-62753221. E-mail: tmfu@pku.edu.cn (T.-M.F.).

ORCID

Lu Xu: 0000-0002-0021-9876

Nga L. Ng: 0000-0001-8460-4765

Notes

The authors declare no competing financial interest.

ACKNOWLEDGMENTS

This work was supported by the Ministry of Science and Technology of China (2017YFC0209802, 2014CB441303), the National Natural Science Foundation of China (41222035, 41461164007), and the Chinese Scholarship Council. L.X. and N.L.N. acknowledge support from US National Science Foundation grant 1455588. The contributions of PNNL authors in this study were supported by the U.S. Department of Energy's Office of Science as part of the Atmospheric System Research (ASR) program and the Regional and Global Climate Modeling Program. The Pacific Northwest National Laboratory is operated for DOE by Battelle Memorial Institute under contract DE-AC05-76RL01830.

REFERENCES

(1) Xu, L.; Kollman, M. S.; Song, C.; Shilling, J. E.; Ng, N. L. Effects of NO_x on the volatility of secondary organic aerosol from isoprene photooxidation. *Environ. Sci. Technol.* **2014**, *48*, 2253−2262.

(2) Ng, N. L.; Kroll, J. H.; Chan, A. W. H.; Chhabra, P. S.; Flagan, R. C.; Seinfeld, J. H. Secondary organic aerosol formation from *m*-xylene, toluene, and benzene. *Atmos. Chem. Phys.* **2007**, *7*, 3909−3922.

(3) Ng, N. L.; Chhabra, P. S.; Chan, A. W. H.; Surratt, J. D.; Kroll, J. H.; Kwan, A. J.; McCabe, D. C.; Wennberg, P. O.; Sorooshian, A.; Murphy, S. M.; Dalleska, N. F.; Flagan, R. C.; Seinfeld, J. H. Effect of NOx level on secondary organic aerosol (SOA) formation from the photooxidation of terpenes. *Atmos. Chem. Phys.* **2007**, *7*, 5159−5174.

(4) Ye, P. L.; Zhao, Y. L.; Chuang, W. K.; Robinson, A. L.; Donahue, N. M. Secondary organic aerosol production from pinanediol, a semivolatile surrogate for first-generation oxidation products of monoterpenes. *Atmos. Chem. Phys.* **2018**, *18*, 6171−6186.

(5) Kroll, J. H.; Ng, N. L.; Murphy, S. M.; Flagan, R. C.; Seinfeld, J. H. Secondary organic aerosol formation from isoprene photooxidation. *Environ. Sci. Technol.* **2006**, *40* (6), 1869−1877.

(6) Surratt, J. D.; Murphy, S. M.; Kroll, J. H.; Ng, N. L.; Hildebrandt, L.; Sorooshian, A.; Szmigielski, R.; Vermeylen, R.; Maenhaut, W.; Claeys, M.; Flagan, R. C.; Seinfeld, J. H. Chemical composition of secondary organic aerosol formed from the photooxidation of isoprene. *J. Phys. Chem. A* **2006**, *110* (31), 9665−9690.

(7) Lane, T. E.; Donahue, N. M.; Pandis, S. N. Simulating secondary organic aerosol formation using the volatility basis-set approach in a chemical transport model. *Atmos. Environ.* **2008**, *42*, 7439−7451.

(8) Stanier, C. O.; Donahue, N.; Pandis, S. N. Parameterization of secondary organic aerosol mass fractions from smog chamber data. *Atmos. Environ.* **2008**, *42*, 2276−2299.

(9) Donahue, N. M.; Epstein, S. A.; Pandis, S. N.; Robinson, A. L. A two-dimensional volatility basis set: 1. Organic-aerosol mixing thermodynamics. *Atmos. Chem. Phys.* **2011**, *11* (7), 3303−3318.

(10) Donahue, N. M.; Henry, K. M.; Mentel, T. F.; Kiendler-Scharr, A.; Spindler, C.; Bohn, B.; Brauers, T.; Dorn, H. P.; Fuchs, H.; Tillmann, R.; Wahner, A.; Saathoff, H.; Naumann, K. H.; Mohler, O.; Leisner, T.; Muller, L.; Reinnig, M. C.; Hoffmann, T.; Salo, K.; Hallquist, M.; Frosch, M.; Bilde, M.; Tritscher, T.; Barmet, P.; Praplan, A. P.; DeCarlo, P. F.; Dommen, J.; Prevot, A. S. H.; Baltensperger, U. Aging of biogenic secondary organic aerosol via gas-phase OH radical reactions. *Proc. Natl. Acad. Sci. U. S. A.* **2012**, *109* (34), 13503−13508.

(11) Cappa, C. D.; Wilson, K. R. Multi-generation gas-phase oxidation, equilibrium partitioning, and the formation and evolution of secondary organic aerosol. *Atmos. Chem. Phys.* **2012**, *12* (20), 9505−9528.

(12) Pankow, J. F. An Absorption-Model of the Gas Aerosol Partitioning Involved in the Formation of Secondary Organic Aerosol. *Atmos. Environ.* **1994**, *28*, 189−193.

(13) Donahue, N. M.; Robinson, A. L.; Stanier, C. O.; Pandis, S. N. Coupled partitioning, dilution, and chemical aging of semivolatile organics. *Environ. Sci. Technol.* **2006**, *40*, 2635−2643.

(14) Ahmadov, R.; Mckeen, S. A.; Robinson, A. L.; Bahreini, R.; Middlebrook, A. M.; de Gouw, J. A.; Meagher, J.; Hsie, E.-Y.; Edgerton, E.; Shaw, S.; Trainer, M. A volatility basis set model for summertime secondary organic aerosols over the eastern United States in 2006. *J. Geophys. Res. Atmos* **2012**, *117*, D06301.

(15) Shrivastava, M.; Zelenyuk, A.; Imre, D.; Easter, R.; Beranek, J.; Zaveri, R. A.; Fast, J. Implications of low volatility SOA and gas-phase fragmentation reactions on SOA loadings and their spatial and temporal evolution in the atmosphere. *J. Geophys. Res. Atmos* **2013**, *118*, 3328−3342.

(16) Shrivastava, M.; Easter, R. C.; Liu, X.; Zelenyuk, A.; Singh, B.; Zhang, K.; Ma, P. L.; Chand, D.; Ghan, S.; Jimenez, J. L.; Zhang, Q.; Fast, J.; Rasch, P. J.; Tiitta, P. Global transformation and fate of SOA: Implications of low-volatility SOA and gas-phase fragmentation reactions. *J. Geophys. Res. Atmos* **2015**, *120*, 4169.

(17) Pathak, P. K.; Presto, A. A.; Lane, T. E.; Stanier, C. O.; Donahue, N. M.; Pandis, S. N. Ozonolysis of α-pinene: parameterization of secondary organic aerosol mass fraction. *Atmos. Chem. Phys.* **2007**, *7*, 3811−3821.

(18) Nguyen, T. B.; Laskin, J.; Laskin, A.; Nizkorodov, S. A. Nitrogen-containing organic compounds and oligomers in secondary organic aerosol formed by photooxidation of isoprene. *Environ. Sci. Technol.* **2011**, *45* (16), 6908−6918.

(19) Ng, N. L.; Kroll, J. H.; Keywood, M. D.; Bahreini, R.; Varutbangkul, V.; Flagan, R. C.; Seinfeld, J. H.; Lee, A.; Goldstein, A. H. Contribution of first- versus second-generation products to secondary organic aerosols formed in the oxidation of biogenic hydrocarbons. *Environ. Sci. Technol.* **2006**, *40* (7), 2283−2297.

(20) St Clair, J. M.; Rivera-Rios, J. C.; Crounse, J. D.; Knap, H. C.; Bates, K. H.; Teng, A. P.; Jørgensen, S.; Kjaergaard, H. G.; Keutsch, F. N.; Wennberg, P. O. Kinetics and products of the reaction of the first-generation isoprene hydroxy hydroperoxide (ISOPOOH) with OH. *J. Phys. Chem. A* **2016**, *120* (9), 1441−1451.

(21) Zhang, X.; Cappa, C. D.; Jathar, S. H.; McVay, R. C.; Ensberg, J. J.; Kleeman, M. J.; Seinfeld, J. H. Influence of vapor wall loss in laboratory chambers on yields of secondary organic aerosol. *Proc. Natl. Acad. Sci. U. S. A.* **2014**, *111*, 5802−5807.

(22) Zhang, X.; Schwantes, R. H.; McVay, R. C.; Lignell, H.; Coggon, M. M.; Flagan, R. C.; Seinfeld, J. H. Vapor wall deposition in Teflon chambers. *Atmos. Chem. Phys.* **2015**, *15*, 4197−4214.

(23) Cappa, C. D.; Jathar, S. H.; Kleeman, M. J.; Docherty, K. S.; Jimenez, J. L.; Seinfeld, J. H.; Wexler, A. S. Simulating secondary organic aerosol in a regional air quality model using the statistical

DOI: 10.1021/acs.est.8b00373
Environ. Sci. Technol. 2018, 52, 9225−9234

oxidation model − Part 2: Assessing the influence of vapor wall losses. *Atmos. Chem. Phys.* **2016**, *16*, 3041−3059.
(24) Nah, T.; McVay, R. C.; Zhang, X.; Boyd, C. M.; Seinfeld, J. H.; Ng, N. L. Influence of Seed Aerosol Surface Area and Oxidation Rate on Vapor-Wall Deposition and SOA Mass Yields: A case study with α-pinene Ozonolysis. *Atmos. Chem. Phys.* **2016**, *16*, 9361−9379.
(25) Kroll, J. H.; Donahue, N. M.; Jimenez, J. L.; Kessler, S. H.; Canagaratna, M. R.; Wilson, K. R.; Altieri, K. E.; Mazzoleni, L. R.; Wozniak, A. S.; Bluhm, H.; Mysak, E. R.; Smith, J. D.; Kolb, C. E.; Worsnop, D. R. Carbon oxidation state as a metric for describing the chemistry of atmospheric organic aerosol. *Nat. Chem.* **2011**, *3* (2), 133−139.
(26) D'Ambro, E. L.; Lee, B. H.; Liu, J.; Shilling, J. E.; Gaston, C. J.; Lopez-Hilfiker, F. D.; Schobesberger, S.; Zaveri, R. A.; Mohr, C.; Lutz, A.; Zhang, Z.; Gold, A.; Surratt, J. D.; Rivera-Rios, J. C.; Keutsch, F. N.; Thornton, J. A. Molecular composition and volatility of isoprene photochemical oxidation secondary organic aerosol under low- and high-NOx conditions. *Atmos. Chem. Phys.* **2017**, *17* (1), 159−174.
(27) Liu, J.; D'Ambro, E. L.; Lee, B. H.; Lopez-Hilfiker, F. D.; Zaveri, R. A.; Rivera-Rios, J. C.; Keutsch, F. N.; Iyer, S.; Kurten, T.; Zhang, Z.; Gold, A.; Surratt, J. D.; Shilling, J. E.; Thornton, J. A. Efficient Isoprene Secondary Organic Aerosol Formation from a Non-IEPDX Pathway. *Environ. Sci. Technol.* **2016**, *50* (18), 9872−9880.
(28) Krechmer, J. E.; Coggon, M. M.; Massoli, P.; Nguyen, T. B.; Crounse, J. D.; Hu, W.; Day, D. A.; Tyndall, G. S.; Henze, D. K.; Rivera-Rios, J. C.; Nowak, J. B.; Kimmel, J. R.; Mauldin, R. L., III; Stark, H.; Jayne, J. T.; Sipila, M.; Junninen, H.; St Clair, J. M.; Zhang, X.; Feiner, P. A.; Zhang, L.; Miller, D. O.; Brune, W. H.; Keutsch, F. N.; Wennberg, P. O.; Seinfeld, J. H.; Worsnop, D. R.; Jimenez, J. L.; Canagaratna, M. R. Formation of Low Volatility Organic Compounds and Secondary Organic Aerosol from Isoprene Hydroxyhydroperoxide Low-NO Oxidation. *Environ. Sci. Technol.* **2015**, *49* (17), 10330−10339.
(29) Zhao, B.; Wang, S.; Donahue, N. M.; Chuang, W.; Ruiz, L. H.; Ng, N. L.; Wang, Y.; Hao, J. Evaluation of one-dimensional and two-dimensional volatility basis sets in simulating the aging of secondary organic aerosol with smog-chamber experiments. *Environ. Sci. Technol.* **2015**, *49* (4), 2245−2254.
(30) Jathar, S. H.; Cappa, C. D.; Wexler, A. S.; Seinfeld, J. H.; Kleeman, M. J. Simulating secondary organic aerosol in a regional air quality model using the statistical oxidation model − Part 1: Assessing the influence of constrained multi-generational ageing. *Atmos. Chem. Phys.* **2016**, *16*, 2309−2322.
(31) Zaveri, R. A.; Easter, R. C.; Fast, J. D.; Peters, L. K. Model for Simulating Aerosol Interactions and Chemistry (MOSAIC). *J. Geophys. Res.* **2008**, *113*, D13204.
(32) Atkinson, R.; Aschmann, S. M. RATE CONSTANTS FOR THE REACTION OF OH RADICALS WITH A SERIES OF ALKENES AND DIALKENES AT 295 ± 1K. *Int. J. Chem. Kinet.* **1984**, *16* (10), 1175−1186.
(33) Donahue, N. M.; Kroll, J. H.; Pandis, S. N.; Robinson, A. L. A two-dimensional volatility basis set − Part 2: Diagnostics of organic-aerosol evolution. *Atmos. Chem. Phys.* **2012**, *12*, 615−634.
(34) Murphy, B. N.; Pandis, S. N. Simulating the formation of semivolatile primary and secondary organic aerosol in a regional chemical transport model. *Environ. Sci. Technol.* **2009**, *43*, 4722−4728.
(35) Zhang, X.; Pandis, S. N.; Seinfeld, J. H. Diffusion-limited versus quasi-equilibrium aerosol growth. *Aerosol Sci. Technol.* **2012**, *46*, 874−885.
(36) Varga, Z.; Kiss, G.; Hansson, H. C. Modelling the cloud condensation nucleus activity of organic acids on the basis of surface tension and osmolality measurements. *Atmos. Chem. Phys.* **2007**, *7*, 4601−4611.
(37) Zaveri, R. A.; Easter, R. C.; Shilling, J. E.; Seinfeld, J. H. Modeling kinetic partitioning of secondary organic aerosol and size distribution dynamics: representing effects of volatility, phase state, and particle-phase reaction. *Atmos. Chem. Phys.* **2014**, *14*, 5153−5181.
(38) Park, S. H.; Lee, K. W. Condensational growth of polydisperse aerosol for the entire particle size range. *Aerosol Sci. Technol.* **2000**, *33*, 222−227.
(39) Kalberer, M.; Paulsen, D.; Sax, M.; Steinbacher, M.; Dommen, J.; Prevot, A. S.; Fisseha, R.; Weingartner, E.; Frankevich, V.; Zenobi, R.; Baltensperger, U. Identification of polymers as major components of atmospheric organic aerosols. *Science* **2004**, *303* (5664), 1659−62.
(40) Cappa, C. D.; Wilson, K. R. Evolution of organic aerosol mass spectra upon heating: Implications for OA phase and partitioning behavior. *Atmos. Chem. Phys.* **2011**, *11* (5), 1895−1911.
(41) Hodzic, A.; Madronich, S.; Kasibhatla, P. S.; Tyndall, G.; Aumont, B.; Jimenez, J. L.; Lee-Taylor, J.; Orlando, J. Organic photolysis reactions in tropospheric aerosols: effect on secondary organic aerosol formation and lifetime. *Atmos. Chem. Phys.* **2015**, *15*, 9253−9269.
(42) Jacobson, M. Z. Development and application of a new air pollution modeling system. Part II: Aerosol module structure and design. *Atmos. Environ.* **1997**, *31*, 131−144.
(43) Jacobson, M. Z.; Turco, R. P.; Jensen, E. J.; Toon, O. B. Modeling coagulation among particles of different composition and size. *Atmos. Environ.* **1994**, *28*, 1327−1338.
(44) Roldin, P.; Eriksson, A. C.; Nordin, E. Z.; Hermansson, E.; Mogensen, D.; Rusanen, A.; Boy, M.; Swietlicki, E.; Svenningsson, B.; Zelenyuk, A.; Pagels, L. Modelling non-equilibrium secondary organic aerosol formation and evaporation with the aerosol dynamics, gas- and particle-phase chemistry kinetic multilayer model ADCHAM. *Atmos. Chem. Phys.* **2014**, *14*, 7953−7993.
(45) Ye, P.; Ding, X.; Hakala, J.; Hofbauer, V.; Robinson, E. S.; Donahue, N. M. Vapor wall loss of semi-volatile organic compounds in a Teflon chamber. *Aerosol Sci. Technol.* **2016**, *50*, 822−834.
(46) Paulot, F.; Crounse, J. D.; Kjaergaard, H. G.; Kurten, A.; St Clair, J. M.; Seinfeld, J. H.; Wennberg, P. O. Unexpected epoxide formation in the gas-phase photooxidation of isoprene. *Science* **2009**, *325* (5941), 730−733.
(47) Bates, K. H.; Crounse, J. D., St.; St Clair, J. M.; Bennett, N. B.; Nguyen, T. B.; Seinfeld, J. H.; Stoltz, B. M.; Wennberg, P. O. Gas phase production and loss of isoprene epoxydiols. *J. Phys. Chem. A* **2014**, *118* (7), 1237−1246.
(48) Surratt, J. D.; Chan, A. W. H.; Eddingsaas, N. C.; Chan, M. N.; Loza, C. L.; Kwan, A. J.; Hersey, S. P.; Flagan, R. C.; Wennberg, P. O.; Seinfeld, J. H. Reactive intermediates revealed in secondary organic aerosol formation from isoprene. *Proc. Natl. Acad. Sci. U. S. A.* **2010**, *107* (15), 6640−6645.
(49) Orlando, J. J.; Tyndall, G. S.; Paulson, S. E. Mechanism of the OH initiated oxidation of methacrolein. *Geophys. Res. Lett.* **1999**, *26* (14), 2191−2194.
(50) Paulot, F.; Crounse, J. D.; Kjaergaard, H. G.; Kroll, J. H.; Seinfeld, J. H.; Wennberg, P. O. Isoprene photooxidation: New insights into the production of acids and organic nitrates. *Atmos. Chem. Phys.* **2009**, *9*, 1479−1501.
(51) Kjaergaard, H. G.; Knap, H. C.; Ornso, K. B.; Jorgensen, S.; Crounse, J. D.; Paulot, F.; Wennberg, P. O. Atmospheric fate of methacrolein. 2. Formation of lactone and implications for organic aerosol production. *J. Phys. Chem. A* **2012**, *116* (24), 5763−5768.
(52) Orlando, J. J.; Tyndall, G. S. Laboratory studies of organic peroxy radical chemistry: an overview with emphasis on recent issues of atmospheric significance. *Chem. Soc. Rev.* **2012**, *41*, 6294−6317.
(53) Hall, W. A.; Johnston, M. V. The Thermal-Stability of Oligomers in Alpha-Pinene Secondary Organic Aerosol. *Aerosol Sci. Technol.* **2012**, *46*, 983−989.
(54) Zaveri, R. A.; Shilling, J. E.; Zelenyuk, A.; Liu, J. M.; Bell, D. M.; D'Ambro, E. L.; Gaston, C. J.; Thornton, J. A.; Laskin, A.; Lin, P.; Wilson, J. M.; Easter, R. C.; Wang, J.; Bertram, A. K.; Martin, S. T.; Seinfeld, J. H.; Worsnop, D. R. Growth kinetics and size distribution dynamics of viscous secondary organic aerosol. *Environ. Sci. Technol.* **2018**, *52* (3), 1191−1199.

DOI: 10.1021/acs.est.8b00373
Environ. Sci. Technol. 2018, 52, 9225−9234